

*Journal of*  
***Mechanics of  
Materials and Structures***

A PLANE STRESS PERFECTLY PLASTIC MODE I CRACK  
PROBLEM FOR A YIELD CONDITION BASED ON THE SECOND  
AND THIRD INVARIANTS OF THE DEVIATORIC STRESS TENSOR

David J. Unger

**Volume 3, Nº 4**

**April 2008**



mathematical sciences publishers



## A PLANE STRESS PERFECTLY PLASTIC MODE I CRACK PROBLEM FOR A YIELD CONDITION BASED ON THE SECOND AND THIRD INVARIANTS OF THE DEVIATORIC STRESS TENSOR

DAVID J. UNGER

A statically admissible solution for the opening mode of fracture under plane stress loading conditions is obtained for a yield condition containing both the second and third invariants of the deviatoric stress tensor. This yield locus lies approximately midway between the Mises and Tresca yield loci in the principal stress plane. The crack problem addressed is analogous to an earlier one investigated by John W. Hutchinson for the Mises yield condition. A stress function approach to the present problem results in a differential algebraic equation rather than an ordinary differential equation as in the former case. It is found that a reduction of order is possible for this second order differential equation of the sixth degree through a simple transformation which generates a Clairaut equation. This equation can be integrated analytically to obtain the general solution of the governing second order differential equation for uniform states of stress. This general solution is applicable to two of three distinct sectors of the plane crack problem. The remaining sector in the plane is governed by the singular solution of this Clairaut equation. The first integral of the singular solution, which is the envelope of general solution, is found through the use of a contact transformation. This transformation aids in reduction of this equation to that of a first order differential equation of the thirtieth degree. The primitive of this first order differential algebraic equation is obtained by numerical solution. An approximate analytical solution to the problem is also provided. These results are compared to those obtained previously for the analogous crack problem under the Mises yield condition.

### 1. Introduction

Drucker [1949; 1962] illustrated the “truly remarkable correlation” of experimental data of an aluminum alloy [Osgood 1947] with a yield condition based upon the second and third invariants of the deviatoric stress tensor. Clearly what appeared to be a sizable band of experimental scatter in a plot of equivalent stress versus octahedral strain, under both the Tresca and Mises yield criteria, became a very narrow locus under this alternative yield condition. Despite the excellent agreement with experimental data, this particular yield condition has been used only rarely in the literature. The probable cause of this avoidance is the yield condition’s mathematical complexity over the Mises yield condition, which is based on the second deviatoric stress invariant alone. However, with today’s widespread availability of both symbolic mathematical and numerical computer software, this particular concern need not be the only deciding factor.

Admittedly, the results obtained here may in fact turn out to be a rather fine point with limited practical significance, as the predictions are very close to those found using the Mises yield condition, while the

---

*Keywords:* plane stress, mode I crack, perfectly plastic yield condition, second third invariants deviatoric stress tensor, differential algebraic equation, DAE.

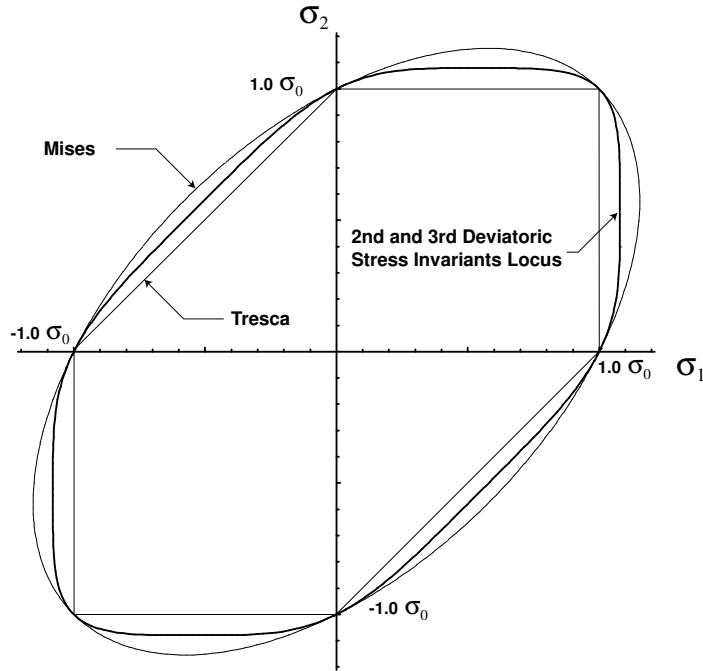


**Figure 1.** Three different yield loci in the principal stress plane.

increase in mathematical difficulty in obtaining solution is enormous. Nevertheless, this analysis contains some interesting and novel mathematical aspects that may aid others in their own research on either yield criteria or on differential algebraic equations (DAE). These include the use of a contact transformation in determining the singular solution of a DAE and the use of a phase plane analysis in determining an approximate singular solution in the form of a Jacobian elliptic function. In this respect there is merit to reporting the results.

The yield condition proposed by Drucker is shown in Figure 1 in the principal stress plane for a state of plane stress loading conditions, where  $\sigma_1$  is the first principal stress and  $\sigma_2$  is the second principal stress ( $\sigma_3 = 0$ ). In terms of the deviatoric stress invariants it assumes the algebraic form

$$(J_2)^3 - (3J_3/2)^2 = (a\sigma_0)^6, \quad (1)$$

where  $J_2$  and  $J_3$  are the second and third invariants of the deviatoric stress tensor, respectively [Chakrabarty 1987], and  $a$  is the proportionality constant<sup>1</sup> between the yield stress in pure shear  $\tau_0$  and the yield stress in tension  $\sigma_0$

$$\tau_0 = a\sigma_0, \quad a = \sqrt[6]{2/81} \approx 0.540. \quad (2)$$

---

<sup>1</sup>This value  $a$  is approximately midway between analogous relationships for the Tresca yield condition 0.500 and the Mises  $\approx 0.577$ .

In polar coordinates, these invariants become explicitly

$$\begin{aligned} J_2 &= \frac{1}{3}(\sigma_r^2 - \sigma_r\sigma_\theta + \sigma_\theta^2) + \tau_{r\theta}^2, \\ J_3 &= \frac{\sigma_r + \sigma_\theta}{3}[\tau_{r\theta}^2 - (1/9)(2\sigma_r - \sigma_\theta)(2\sigma_\theta - \sigma_r)], \end{aligned} \quad (3)$$

where  $\sigma_r$  and  $\sigma_\theta$  are the normal stresses in the radial and transverse directions respectively and  $\tau_{r\theta}$  is the shear stress.

Drucker [1949] and Freudenthal and Geiringer [1958] introduce this yield condition Equation (1) as being the simplest possible form containing both the second and third deviatoric stress invariants, although neither reference indicates its priority.

## 2. General and singular solutions

By introducing a plastic stress function  $\phi(r, \theta)$  in polar form

$$\phi(r, \theta) = r^2 f(\theta), \quad (4)$$

the stresses derived from it [Unger 2005; 2007]

$$\sigma_\theta = 2f(\theta), \quad (5)$$

$$\tau_{r\theta} = -f'(\theta) = -p, \quad (6)$$

$$\sigma_r = f''(\theta) + 2f(\theta) = p \frac{dp}{df} + 2f, \quad (7)$$

will automatically satisfy the equilibrium equations in the plane, where the number of prime symbols applied to the function  $f(\theta)$  indicate the order of differentiation with respect to  $\theta$ . By substituting Equations (5)–(7) into Equation (3) and subsequently substituting those results into Equation (1), the governing differential equation for the stress function becomes

$$(q^2 - 6fq + 6Q)^3 - (1/12)q^2(2q^2 - 18fq + 18Q)^2 = (2/3)\sigma_0^6, \quad (8)$$

where for brevity the following notation has been adopted in Equation (8)

$$Q = p^2/2 + 2f^2, \quad q = dQ/df. \quad (9)$$

Equation (8) has the form of a Clairaut differential equation [Zwillinger 1989, pp. 150–160]. As such, a Clairaut operator  $U(f)$  may be defined as

$$U = f dQ/df - Q(f) = fq - Q, \quad (10)$$

which brings Equation (8) into the form

$$3(q^2 - 6U)^3 - q^2(q^2 - 9U)^2 = 2\sigma_0^6. \quad (11)$$

The operational procedure to solve a Clairaut equation is to substitute a constant in place of the first derivative of the dependent variable with respect to the independent variable and to solve for the dependent variable. The dependent variable constitutes the solution of the problem.

In this case  $q$  will be set equal to  $c$  with  $Q$  being identified temporarily as the dependent variable, which is a function of  $f$ . Solving Equation (11) for  $U(f)$  and substituting Equation (10) into the result, one finds that

$$Q(f) = cf - \frac{c^2}{8} + \frac{5c^4}{24 \cdot 3^{1/3}} \frac{1}{M(c, \sigma_0)} - \frac{M(c, \sigma_0)}{24 \cdot 3^{2/3}}, \quad (12)$$

where the constant  $M(c, \sigma_0)$  is defined in terms of the two other parameters as

$$M(c, \sigma_0) = \left[ 3c^6 - 192\sigma_0^6 + 8\sqrt{6} \sqrt{c^{12} - 3c^6\sigma_0^6 + 96\sigma_0^{12}} \right]^{1/3}. \quad (13)$$

Reintroducing the fundamental definition of  $Q$  from Equation (9), one may now separate variables and integrate to obtain the following branch of the general solution of Equation (8)

$$f(\theta) = \frac{c}{4} - \frac{1}{4 \cdot 3^{2/3}} \sqrt{\frac{5c^4}{M(c, \sigma_0)} - \frac{M(c, \sigma_0)}{3^{1/3}}} \sin(2\theta + \alpha), \quad (14)$$

where  $\alpha$  represents the second constant of integration.

An additional solution to that of Equation (14) exists for Equation (8) in the form of a singular solution. The singular solution of Equation (8) represents the envelope of the family of ellipses that Equation (14) will generate in the phase space  $(f, p)$  upon varying the parameter  $c$  (the choice of parameter  $\alpha$  is immaterial). It cannot be obtained directly from Equation (14) by simply selecting particular values of the constants  $c$  or  $\alpha$ .

The conventional approach to obtaining a singular solution of a Clairaut equation is to first separate the governing equation into a function of the Clairaut operator, represented here by  $U$ , and a function of the first derivative  $q$ . By differentiating this expression with respect to the independent variable  $f$ , a pair of simultaneous equations results from which the first derivative can be eliminated to obtain a solution [Zwillinger 1989].

However, in the present situation obtaining the function of  $U$  requires a solution of a cubic algebraic equation which is cumbersome.

As an alternative, a solution technique described in [Ince 1956], as the principal of duality, will be used here. To achieve solution, expand the parenthetical expressions in Equation (11) and rewrite the expansion as follows, using the fundamental definition of  $U$

$$2q^6 - 36q^4(fq - Q) + 243q^2(fq - Q)^2 - 648(fq - Q)^3 = 2\sigma_0^6. \quad (15)$$

Next, make the following substitutions for the variables appearing in Equation (15)

$$f = P, \quad Q = XP - Y, \quad q = X, \quad (16)$$

where  $P$  is defined as the first derivative of the new dependent variable  $Y$  with respect to the new independent variable  $X$

$$P = dY/dX. \quad (17)$$

Upon substitution of the variables defined by Equations (16) into Equation (15), one converts the differential equation into the following algebraic equation

$$2X^6 - 36X^4Y + 243X^2Y^2 - 648Y^3 = 2\sigma_0^6. \quad (18)$$

By differentiating Equation (18) with respect to  $X$  and by employing the definition of  $P$ , one finds upon solving the expression for  $P$  that

$$P = X \frac{24X^2Y - 2X^4 - 81Y^2}{81X^2Y - 6X^4 - 324Y^2}. \quad (19)$$

Now the inverse of the contact transformation, Equation (16), is given by

$$X = q, \quad Y = fq - Q, \quad P = f. \quad (20)$$

By transforming Equation (19) back to the original variables one finds that

$$f = q \frac{24q^2(fq - Q) - 2q^4 - 81(fq - Q)^2}{81q^2(fq - Q) - 6q^4 - 324(fq - Q)^2}. \quad (21)$$

Eliminating the common variable  $q$  between Equations (15) and (21), and then substituting the definition for  $Q$  from Equation (9) into the result, one reduces the order of the governing equation for the singular solution by one to:

$$\begin{aligned} & 387420489(4f^2 + p^2)^{12}[8f^6 + 51f^4p^2 + 24f^2p^4 + 8p^6] \\ &= 28697814(4f^2 + p^2)^6[33280f^{12} + 163680f^{10}p^2 + 16800f^8p^4 - 17536f^6p^6 \\ &\quad - 16239f^4p^8 - 2136f^2p^{10} + 88p^{12}] \sigma_0^6 \\ &- 11337408[8783360f^{18} + 30758400f^{16}p^2 + 2053440f^{14}p^4 \\ &\quad + 4665120f^{12}p^6 - 2198394f^{10}p^8 + 352476f^8p^{10} \\ &\quad - 147783f^6p^{12} + 127980f^4p^{14} - 4986f^2p^{16} + 80p^{18}] \sigma_0^{12} \\ &+ 1492992[598880f^{12} + 436800f^{10}p^2 + 53400f^8p^4 - 25322f^6p^6 \\ &\quad + 29955f^4p^8 - 6153f^2p^{10} + 110p^{12}] \sigma_0^{18} \\ &- 442368[2120f^6 + 600f^4p^2 - 435f^2p^4 + 32p^6] \sigma_0^{24} + 262144\sigma_0^{30}, \end{aligned} \quad (22)$$

where  $p$  is the first derivative of the function  $f$  with respect to  $\theta$ , as in Equation (6).

This result, which is tedious to do by hand, was determined using the command function *Eliminate* of Mathematica®.

A plot of Equation (22) is shown in Figure 2 for the first quadrant of the phase plane. The insert in figure reveals that the complete locus of Equation (22) is barrel shaped; nearly flat on the top and bottom, with curved lateral sides. The complete locus is shown inscribed within a circle representing the locus of the Mises singular solution [Unger 2005].

Note that Equation (22) provides an exact relationship between stresses  $\tau_{r\theta}$  and  $\sigma_\theta$  of the singular solution once the associated relationships between the stress function  $f$  and its first derivative  $p$ , such that Equations (5) and (6), are substituted into that equation. In Figure 3, this relationship is plotted as  $\tau_{r\theta}$  versus  $\sigma_\theta$  which generates an oval shape. An implicit plotting routine is required to find and draw the locus of this thirtieth order algebraic relationship.

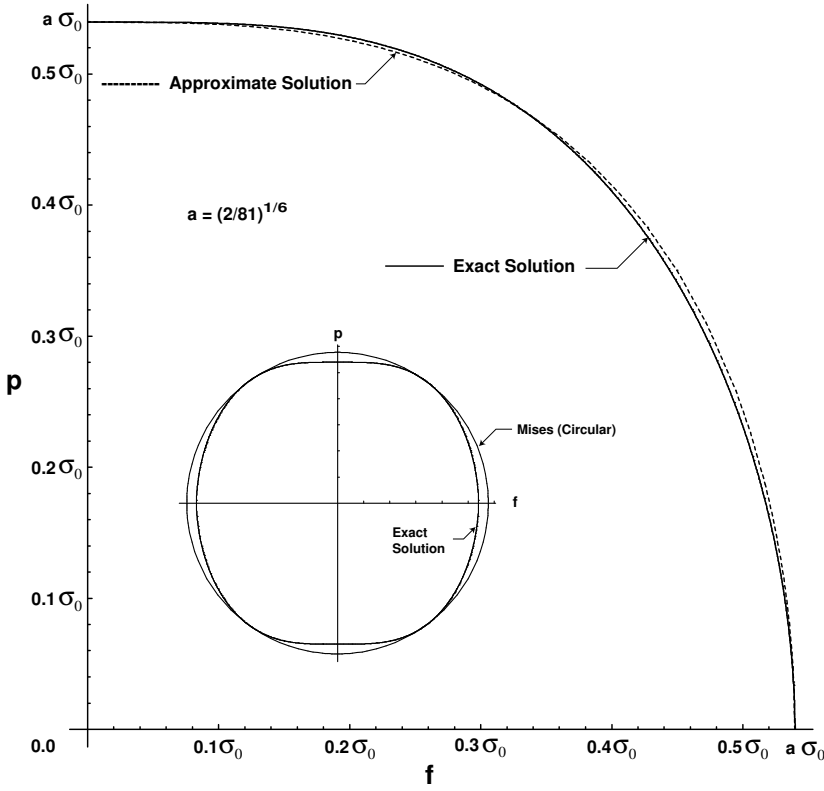


**Figure 2.** Phase plane analysis of the singular solution Equation (22), its approximation Equation (25), and the analogous Mises solution.

Now, by eliminating the common terms in parentheses  $f q - Q$  from Equations (15) and (21), one obtains an expression that relates the remaining functions  $f$  and  $q$ . The function  $f$  is one half the value of  $\sigma_\theta$  by Equation (5). In addition, one can relate  $q$  to the sum of the normal stresses as

$$q = p \frac{dp}{df} + 4f = \sigma_r + 2f = \sigma_r + \sigma_\theta, \quad (23)$$

by using Equations (5), (7) and (9). Thus an exact relationship can be determined between the stresses  $\sigma_r$  and  $\sigma_\theta$  of the singular solution as

$$\begin{aligned} 32\sigma_r^{15} + 336\sigma_r^{14}\sigma_\theta + 1587\sigma_r^{13}\sigma_\theta^2 + 4453\sigma_r^{12}\sigma_\theta^3 + 8274\sigma_r^{11}\sigma_\theta^4 + 10758\sigma_r^{10}\sigma_\theta^5 \\ + 9977\sigma_r^9\sigma_\theta^6 + 6039\sigma_r^8\sigma_\theta^7 + 396\sigma_r^7\sigma_\theta^8 - 4972\sigma_r^6\sigma_\theta^9 - 7755\sigma_r^5\sigma_\theta^{10} - 6909\sigma_r^4\sigma_\theta^{11} \\ - 3998\sigma_r^3\sigma_\theta^{12} - 1482\sigma_r^2\sigma_\theta^{13} - 321\sigma_r\sigma_\theta^{14} - 31\sigma_\theta^{15} - 32\sigma_r^9\sigma_\theta^6 + 144\sigma_r^8\sigma_\theta\sigma_0^6 \\ + 1575\sigma_r^7\sigma_\theta^2\sigma_0^6 + 4791\sigma_r^6\sigma_\theta^3\sigma_0^6 + 7767\sigma_r^5\sigma_\theta^4\sigma_0^6 + 7983\sigma_r^4\sigma_\theta^5\sigma_0^6 + 5709\sigma_r^3\sigma_\theta^6\sigma_0^6 \\ + 2925\sigma_r^2\sigma_\theta^7\sigma_0^6 + 981\sigma_r\sigma_\theta^8\sigma_0^6 + 157\sigma_\theta^9\sigma_0^6 + 1944\sigma_r^3\sigma_0^{12} - 5832\sigma_r^2\sigma_\theta\sigma_0^{12} \\ + 5832\sigma_r\sigma_\theta^2\sigma_0^{12} - 1944\sigma_\theta^3\sigma_0^{12} = 0. \end{aligned} \quad (24)$$

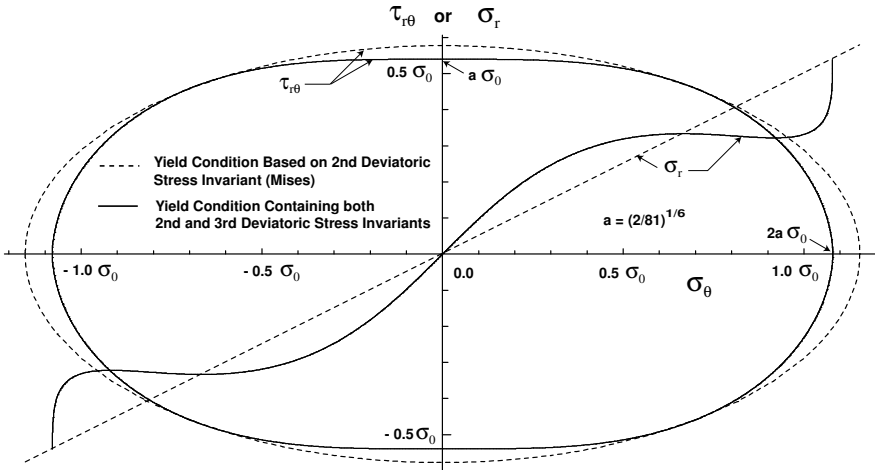


**Figure 3.** Exact relationships among stresses for the singular solutions of two different yield conditions.

This relationship appears as an open curve when plotted in Figure 3.

The continuous curves in Figure 3 constitute exact relationships among the stresses for the singular solution of Equation (8), and consequently satisfy yield condition, Equation (1). For comparison, the analogous stresses for the Mises yield condition are also plotted using dashed line segments. The greatest difference between the two different yield criteria is in  $\sigma_r$  which is a straight line in the case of the Mises yield condition and a curve in case of yield condition, Equation (1). The plots of  $\sigma_r$  as a function of  $\sigma_\theta$  reveal two distinct ovals for the two different yield criteria. In the case of the Mises yield condition, this oval is also an ellipse.

### 3. Analytical approximation to the singular solution

The form of the differential algebraic equation, Equation (22), for the singular solution appears to be insoluble by exact techniques. Consequently, approximate analytical and numerical methods will be used for evaluation.

One approximation of the exact locus Equation (22), but much simpler in form, is given by

$$\left(\frac{P_{\text{approx}}}{a\sigma_0}\right)^2 + \left(\frac{f_{\text{approx}}}{a\sigma_0}\right)^3 = 1. \quad (25)$$

The closeness of fit between the approximate and exact loci in the phase plane is shown in Figure 2. The simplicity of Equation (25) also allows its exact primitive  $f_{\text{approx}}$  to be found as a solution of an ordinary differential equation. This solution will serve as a useful analytical approximation to the solution of Equation (22).

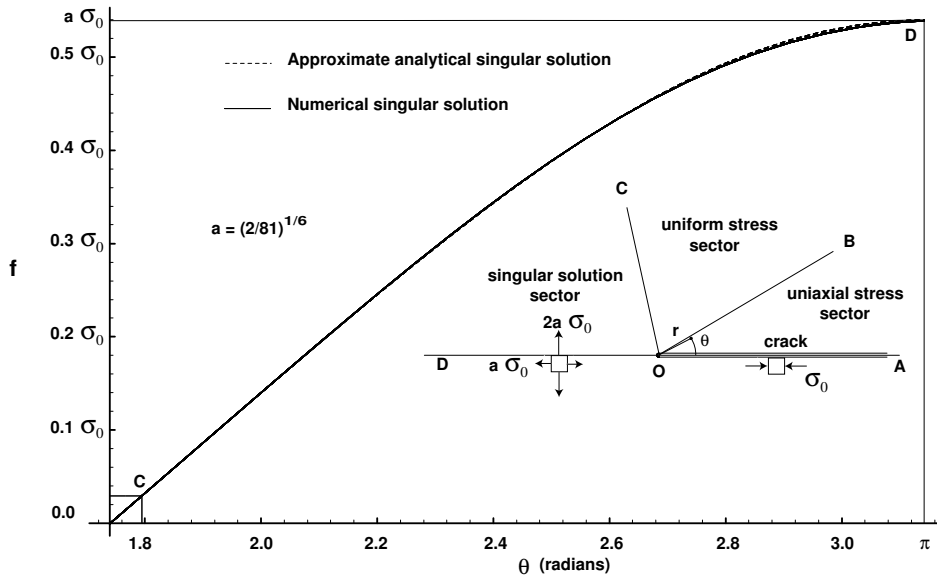


**Figure 4.** Comparison of the numerical singular solution to the analytical approximation, Equation (29).

The variables of the approximate relationship Equation (25) can be separated and integrated to generate the following relationship

$$\theta + \beta = \int_g^1 \frac{du}{\sqrt{1-u^3}}, \quad g = \frac{f_{\text{approx}}}{a\sigma_0}, \quad (26)$$

where  $\beta$  is a constant of integration.

The remaining integral in Equation (26) can be evaluated using [Gradshteyn and Ryzhik 1980, table entry 3.139 2]. It is represented below as an incomplete elliptic integral of the first kind  $F( , )$ , as in

$$\theta + \beta = \frac{1}{\sqrt[4]{3}} F(\psi, k), \quad \psi = \cos^{-1} \frac{\sqrt{3}-1+g}{\sqrt{3}+1-g}, \quad k = \sin 75^\circ, \quad (27)$$

where the incomplete elliptic integral  $F( , )$  is defined below as [Gradshteyn and Ryzhik 1980, relationship 8.111 2]

$$F(\psi, k) = \int_0^\psi \frac{dx}{\sqrt{1-k^2 \sin^2 x}}. \quad (28)$$

Upon inversion of the elliptic integral appearing in Equation (27), one obtains after simplification that

$$f_{\text{approx}} = a\sigma_0 - \sqrt{3}a\sigma_0 \frac{1 - cn\sqrt[4]{3}(\theta + \beta)}{1 + cn\sqrt[4]{3}(\theta + \beta)}, \quad (29)$$

where  $cn( )$  is a Jacobian cosine-amplitude elliptic function of modulus  $k$ . The particular value of  $k$  for use in this approximate solution is given in Equation (27).

The function  $f_{\text{approx}}$  provides a close approximation to the exact relationship between  $f$  and  $\theta$ , when compared to results from a numerical solution, which are plotted in Figure 4. However, the approximate analytical solution should not be used for the direct determination of  $\sigma_r$  by Equation (7), as this would require taking the second derivative of the function with respect to the angle  $\theta$ . Accuracy cannot be guaranteed by this procedure, nor will the yield condition be satisfied in general by the derived stresses.

Instead, an alternative method of stress evaluation is proposed which will ensure that the yield condition is satisfied.

A good approximation to the singular solution can be obtained by using Equation (29) to obtain an approximate relationship between  $f$  and  $\theta$  from which one uses Equation (5) to obtain  $\sigma_\theta$  as a function of  $\theta$ . The same relationships used previously to generate stresses  $\tau_{r\theta}$  and  $\sigma_r$  as functions of  $\sigma_\theta$  in Figure 3 can then be used to generate a stress field that satisfies yield condition Equation (1) for any given angle  $\theta$ .

#### 4. Crack problem

A schematic diagram of the basic crack geometry is shown in the insert of Figure 4. The domain is composed of three distinct sectors which cover the upper half plane  $0 \leq \theta \leq \pi$ . The semiinfinite crack is positioned along the coordinate  $\theta = 0$ . Two angles,  $\theta_{AOB}$  and  $\theta_{AOC}$ , mark the divisions between the three sectors. These angles are measured counterclockwise from the crack line  $OA$  to rays  $OB$  and  $OC$ , respectively. Using symmetry, the solution for the lower half plane can be inferred from the solution of the upper half plane.

A dedicated computer program was written to solve the mode I perfectly plastic crack problem for the upper half plane under yield condition, Equation (1).

The code assumes a uniaxial state of compression in sector  $AOB$ . The stress function applicable to region  $OAB$  is obtained by substituting the following parameters into Equation (14)

$$c = -\sigma_0, \quad \alpha = \frac{3\pi}{2}. \quad (30)$$

The associated stress function assumes the simple form

$$f_{AOB} = -\frac{\sigma_0}{2} \sin^2 \theta, \quad 0 \leq \theta < \theta_{AOB}, \quad (31)$$

after an elementary trigonometric identity has been introduced. This stress function generates a state of compression of magnitude  $\sigma_0$  in region  $AOB$  and meets the traction-free boundary condition along the crack surface  $OA$  as depicted in Figure 4.

Equilibrium requires that both the stress functions and their normal derivatives be continuous across sector boundaries. An iterative process in the software determines the angles from crack line  $OA$  to rays  $OB$  and  $OC$  as

$$\theta_{AOB} = 0.53360 = 30.573^\circ, \quad \theta_{AOC} = 1.79229 = 102.69^\circ. \quad (32)$$

The values of the parameters of Equation (14) for the middle sector  $BOC$  are found simultaneously as

$$c = 0.11383 \sigma_0, \quad \alpha = -0.44270. \quad (33)$$

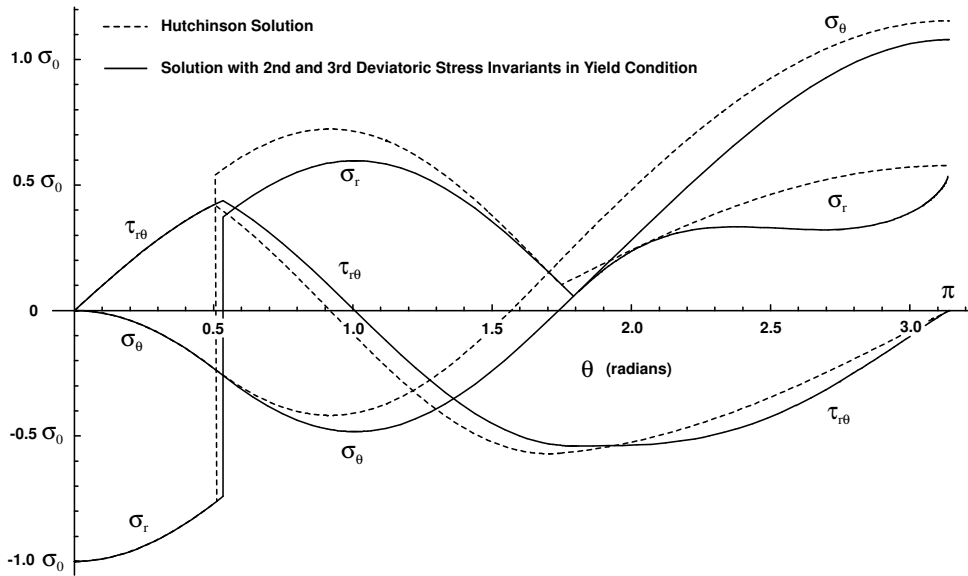


**Figure 5.** Comparison of perfectly plastic stress fields of the mode I fracture problem.

With these constants and Equation (14), one determines the state of stress in sector  $BOC$  using Equations (5)–(7).

The approximate singular solution Equation (29) with  $\beta = -\pi$  is used to relate the angle  $\theta$  to the function  $f$  in the leading sector  $COD$ . The exact stresses, which were plotted previously in Figure 3, can be parametrized in terms of the stress function  $f$ . As these stresses satisfy the yield condition exactly, the error introduced by this procedure is limited to the approximate correlation of  $f$  to  $\theta$ . The numerical data of Figure 4 suggest that the differences are small. See the Appendix for details on the numerical singular solution.

The stresses obtained from this analysis are plotted in Figure 5 as solid curves. Note that a stress discontinuity exists in  $\sigma_r$  at the boundary between regions  $AOB$  and  $BOC$ , as with ray  $OB$  of Figure 4.

The use of the exact relationships among singular solution stresses, as plotted in Figure 3, are necessary in order to duplicate the results shown in Figure 5. In this respect, the author found it computationally expedient to solve the problem with a continuous exact stress  $\sigma_r$  and stress function  $f$  at the second interface  $\theta_{AOC}$ , rather than relying on the continuity of the stress function and its normal derivative  $p$ . The original computational scheme, which did not employ this logic, seemed relatively insensitive to small changes in the interface angle  $\theta_{AOC}$ . This response was related to the nearly constant slope  $p$  of the stress function in this region. As a consequence, a small stress discontinuity in  $\sigma_r$  formed at the interface  $\theta_{AOC}$ , which was unexpected. However, upon implementation of the alternative computational scheme, the stress discontinuity was eliminated leaving the stress function  $f$ , its normal derivative  $p$ , and the normal stress  $\sigma_r$  continuous at the second interface  $\theta_{AOC}$ .

In [Hutchinson 1968] a statically-admissible solution for a perfectly plastic material under the Mises yield condition was obtained for a traction-free semiinfinite mode I crack under plane stress loading conditions. The stress field of Hutchinson for the Mises yield condition is plotted in Figure 5 as dashed

lines. A stress discontinuity exists in normal stress  $\sigma_r$  on the boundary between the trailing sectors as previously noted for yield condition, Equation (1). In the region adjacent to the crack, the stresses are identical for the two different yield criteria. Consequently the dashed line representation of the Hutchinson solution is indiscernible in the portion of the figure where it has been overdrawn by the solid curve. The analogous value of the parameter  $a$  multiplying normal stresses ahead of the crack in Figure 4 is  $1/\sqrt{3}$  for the Mises yield condition.

In Hutchinson [1968], the crack was oriented to the left of the crack tip rather than to the right as illustrated in Figure 4. This reflection of the semiinfinite crack about the vertical axis through the origin O allows for a less congested plot of the three stresses  $\sigma_r$ ,  $\sigma_\theta$ , and  $\tau_{r\theta}$  as functions of the angle  $\theta$ . This is particularly true when two different solutions are superposed on the same graph as they are in Figure 5.

## 5. Conclusions

There are relatively few perfectly plastic solutions for the mode I crack problem using yield criteria other than the traditional Mises (see Unger [2007] for one example). In fact, the second most commonly used yield criterion for metals, the Tresca, does not even admit a concentrated fan of mathematical characteristics under plane stress loading conditions from which one could determine an analogous mode I solution to Hutchinson's [Unger 2005]. Thus, while the predictions of the Mises and Tresca yield conditions are often similar in nature, this conclusion cannot be universally drawn. In a similar light, the behavior of yield condition Equation (1), as it pertains to crack problems, was unknown before the present analysis.

As noted in the previous section, a number of similarities exist between the statically admissible stress fields of the mode I fracture problem under the Mises yield condition and under the alternative yield condition, Equation (1). In the case of Equation (1), the smoothness of this yield surface in the principal stress plane is the likely source of its good correlation with the Mises. In contrast, the Tresca is only piecewise smooth.

What stands out between Hutchinson's mode I solution and the present analysis is the rapid rise in the slope of  $\sigma_r(\theta)$  as  $\theta \rightarrow \pi$  for the solution based on yield condition, Equation (1). Just the opposite behavior is exhibited in Figure 5 for the solution based on the Mises yield condition where the slope of  $\sigma_r(\theta)$  tends to zero as  $\theta \rightarrow \pi$ . One might expect for microstructural defects driven by hydrostatic stress gradients, that this difference might have a significant effect on any mathematical model describing their distribution near the crack tip.

Nevertheless, it is anticipated that in general a slightly better fit of experimental data by Equation (1) will not compensate for its increased complexity over the conventional Mises yield condition.

## Appendix A: Numerical evaluation of the singular solution

The validity of the approximate solution  $f_{\text{approx}}$  is supported by the data shown in Figure 4, where a numerical solution of Equation (22) is compared to the approximate solution Equation (29). In Equation (29) the phase angle  $\beta$  of the function  $cn(\cdot)$  was chosen as

$$\beta = -\pi \quad (\text{A.1})$$

in order to meet boundary conditions on traction for a crack oriented as shown in the insert of Figure 4. With this particular value of  $\beta$ , the function  $cn\sqrt{3}(\theta + \beta)$  evaluates to one at  $\theta = \pi$ , and consequently by Equation (29) the function  $f_{\text{approx}} = a\sigma_0$ . By substituting this particular value for  $f_{\text{approx}}$  into Equation (25), one finds the corresponding value of  $p_{\text{approx}}$  is zero. Collectively these values of  $f_{\text{approx}}$  and  $p_{\text{approx}}$  evaluated at  $\theta = \pi$  fulfill the boundary conditions on traction directly ahead of the crack tip. Correspondingly, along ray  $OD$  of Figure 4 the normal stress  $\sigma_\theta$  has a value of  $2a\sigma_0$  and the shear stress  $\tau_{r\theta}$  has a value of zero.

The initial condition for the numerical evaluation of Equation (22) is

$$f(\theta)|_{\theta_0} = f_0(1.7394) = 0, \quad (\text{A.2})$$

where the value of the initial angle 1.7394 is near to the location where the function  $f_{\text{approx}} = 0$  with phase angle  $\beta$  given by Equation (A.1). The range on the independent variable for the numerical solution of  $f$  will be  $1.7394 \leq \theta \leq \pi$ , which spans approximately one quarter of the function's period.

At first glance it may seem more logical to start the numerical marching scheme at  $\theta = \pi$ , taking the initial value of the function  $f_0$  as  $a\sigma_0$  (to fulfill the boundary condition) and using negative increments in the angle  $\theta$  over the desired range. However, one can prove by direct substitution that  $f = a\sigma_0 = \text{const}$  is an exact solution to Equation (22). Consequently any numerical scheme initiated with this particular value of  $f_0$  will generate this solution regardless of the starting position  $\theta_0$ . Other solutions of Equation (22) having initial data near to the value  $a\sigma_0$ , but differing slightly, will prove computationally unstable. Because of these difficulties the alternative numerical scheme cited was adopted.

The solutions  $f = \pm a\sigma_0$  to Equation (22) are also singular solutions, but of a different classification than the periodic singular solution. They are extraneous solutions because they violate the yield condition. They represent mathematically the envelope (upper and lower bounds respectively) of the periodic singular solution.

The command function *NDSolve* in Mathematica 5.2 was used to solve the associated differential algebraic Equation (22), subject to the initial condition, Equation (A.2). The difference between the numerical solution of Equation (22), subject to the initial condition (A.2), and the approximate analytical solution, Equation (29), with  $\beta$  given in Equation (A.1), is nearly indistinguishable in the plot of these two functions in Figure 4.

See Zwillinger [1989] for a short discussion and additional references on differential algebraic equations and their solution.

### Acknowledgements

The author thanks Dr. Robert A. Clark, Director of the Institute for Global Enterprises in Indiana, and the other members of the Deans' Council of the University of Evansville for his appointment as a U. E. Global Scholar for 2007-2008. The software purchased under this program's professional development budget was essential to the successful completion of this project.

### References

[Chakrabarty 1987] J. Chakrabarty, *Theory of plasticity*, McGraw-Hill, New York, 1987.

- [Drucker 1949] D. C. Drucker, "Relationship of experiments to mathematical theories of plasticity", *J. Appl. Mech. (Trans. ASME)* **16** (1949), 349–357.
- [Drucker 1962] D. C. Drucker, "Basic concepts", Chapter 46, pp. 46–1–46–15 in *Plasticity and viscoelasticity*, edited by W. Flügge, Handbook of Engineering Mechanics, McGraw-Hill, New York, 1962.
- [Freudenthal and Geiringer 1958] A. M. Freudenthal and H. Geiringer, "The mathematical theories of the inelastic continuum, elasticity and plasticity", pp. 282–283 in *Handbuch der physik*, vol. VI, edited by S. Flügge, Springer-Verlag, Berlin, 1958.
- [Gradshteyn and Ryzhik 1980] I. S. Gradshteyn and I. M. Ryzhik, *Table of integrals, series, and products*, Academic Press, New York, 1980.
- [Hutchinson 1968] J. W. Hutchinson, "Plastic stress and strain fields at a crack tip", *J. Mech. Phys. Solids* **16**:5 (1968), 337–342.
- [Ince 1956] E. L. Ince, *Ordinary differential equations*, Dover, New York, 1956.
- [Osgood 1947] W. R. Osgood, "Combined-stress tests on 24S-T aluminum alloy tubes", *J. Appl. Mech. (Trans. ASME)* **14** (1947), 147–153.
- [Unger 2005] D. J. Unger, "A plane stress perfectly plastic mode I crack solution with continuous stress field", *J. Appl. Mech. (Trans. ASME)* **72**:1 (2005), 62–67.
- [Unger 2007] D. J. Unger, "A complete perfectly plastic solution for the mode I crack problem under plane stress loading conditions", *J. Appl. Mech. (Trans. ASME)* **74**:3 (2007), 586–589.
- [Zwillinger 1989] D. Zwillinger, *Handbook of differential equations*, Academic Press, Boston, 1989.

Received 11 Nov 2007. Revised 29 Feb 2008. Accepted 6 Mar 2008.

DAVID J. UNGER: du2@evansville.edu

Department of Mechanical and Civil Engineering, University of Evansville, 1800 Lincoln Avenue, Evansville, IN 47722, United States

